J Solid State Electrochem (2006) 10: 211–222
DOI 10.1007/s10008-005-0665-7

ORIGINAL PAPER

G. Patermarakis

Aluminium anodising in low acidity sulphate baths: growth mechanism and nanostructure of porous anodic films

Received: 17 September 2004 / Revised: 24 November 2004 / Accepted: 10 March 2005 / Published online: 6 August 2005

Abstract Overall kinetic and chronopotentiometric studies were performed during Al anodising in H_2SO_4, 0–5% w/v, bath solutions pure and saturated by $Al_2(SO_4)_3$. Peculiarities in film growth mechanism and nanostructure in these cases appeared, like significant differences of porosity and its dependence on film thickness, different critical current density above which pitting appears, salt deposition on pitted surface regions in saturated bath, etc. The different conditions inside pores are responsible for this behaviour like almost depletion of H^+ during a long initial transient stage in the first case, supersaturation and formation of $Al_2(SO_4)_3$ nanoparticle micelles on pore surface in the second case, etc. Differences in film growth mechanism also appeared between these and alike baths at higher acidity. Anodising in low acidity saturated baths shows superiority for growing low porosity films at specific conditions. New technologies may be suggested to produce optimal films of desired structure.

Keywords Porous anodic aluminas · Low acidity sulphate baths · Chronopotentiometry and overall kinetics · Growth mechanism and nanostructure · Interface colloidal $Al_2(SO_4)_3$

Nomenclature

$a_{H+,\,0}$	Activity of H^+ in the bath bulk solution
$a_{H+,\,x}$	Activity of H^+ in the pore filling solution at distance x from the film surface
$a_{H+,\,b}$	Activity of H^+ in the pore filling solution at pore bases
A	Dimensionless factor equal to $(kjt - m)(4^{-1}\pi S_g d_c k' t)^{-1}$
A_0	nD_b^2
A_1 and A_2	Parameters derived by fitting the equation $A = A_0 + A_1 t + A_2 t^2$ to the experimental results A versus t
A'_1 and A'_2	Parameters derived by fitting the equation $A = A_0 + A_1 h + A_2 h^2$ to the experimental results A versus h
B	Appearance of burning regions on the surface, i.e. advanced, dark colour, black pitting
$C_{a,0}$	Concentration of H_2SO_4 in the bath bulk solution
$C'_{a,0}$	Concentration of H_2SO_4 in the bath bulk solution just exceeding 5% w/v where the j_c becomes identical for both solutions of pure H_2SO_4 and saturated by $Al_2(SO_4)_3$
$C_{a,x}$	Concentration of H_2SO_4 in the pore filling solution at distance x from the film surface
$C_{a,b}$	Concentration of H_2SO_4 at pore bases
$C_{H+,0}$	Concentration of H^+ in the bath bulk solution
$C_{H+,x}$	Concentration of H^+ in the pore filling solution at distance x from the film surface
$C_{H+,b}$	Concentration of H^+ at pore bases
$C_{s,0}$	Concentration of $Al_2(SO_4)_3$ in the bath bulk solution
$C_{s,x}$	Concentration of $Al_2(SO_4)_3$ in the pore filling solution at distance x from the film surface
$C_{s,b}$	Concentration of $Al_2(SO_4)_3$ at pore bases
$C_{s,s}$	Saturation concentration of $Al_2(SO_4)_3$ in the bath bulk solution
d.	Dense H_2SO_4 (95–97% w/w)
d_c	Density of the compact pore wall oxide, 3.42 g cm^{-3}
D_b	Pore base diameter
D_x	Pore diameter at distance x from the film surface
D_c	Cell width

G. Patermarakis
School of Chemical Engineering,
Department of Materials Science and Engineering,
National Technical University, Iroon Polytechniou 9, Zografou, Athens, 157 80, Greece
E-mail: gpaterma@central.ntua.gr
Tel.: +30-210-7723099
Fax: +30-210-7723184

ΔV	Anodising voltage
$\Delta V'_m$	Minimum value of ΔV attained after the initial short transient stage in a time of the order of 1 min
ΔV_m	Minimum value of ΔV attained within the quasi-steady state stage of film growth in saturated baths in a time of the order of ten or of some tens min
h	Film thickness
j	Current density
j_c	Critical current density above which pitting appears
k	Constant for oxide production resulting from Faraday's law
k''	Constant, 3.09×10^{-6} cm^3 mA^{-1} min^{-1}
k'	$k''j$
m	Mass of oxide spread over the whole anodised geometric surface area of Al specimens
n	Surface density of pores
p	Porosity v/v
pH_{in}	pH of solution before anodising
pH_{fi}	pH of solution after each anodising run in each separate condition at one or different anodising times
P	Appearance of pitting regions on the surface
r_x	Rate of pore wall oxide dissolution reaction at distance x from the film surface
S	Development of salt deposit layer on the pitted or burnt surface regions
S_g	Geometric surface area of Al specimens, 30.75 cm^2
T	Bath temperature
T_x	Temperature inside the pores at distance x from the film surface
T_b	Temperature inside the pores around their bases
t	Time of anodising
t_l	Time up to which film thickness increases linearly with time
t_m	Time at which the maximum pore diameter near or at film surface approaches first the cell width that is $t_m \leq t_l$
t_c	Time at which a quasi-steady state maximum limiting h or m is first established

Introduction

The porous anodic alumina films are important materials applied to improve the mechanical properties of Al [1], as anti-corrosion [2–4] and decorating [2, 3] coatings and membranes [5], in magnetic memories [6], catalysis [7–13], nuclear reactors [14], re-chargeable batteries [15], as templates for synthesising emitters [16, 17], etc. Due to their nanometer scale porous structure [2, 3, 7–13] and sizes of particles constituting the pore wall material [18] recently, they have found application in nanoscience and nanotechnology, e.g. forms for electroplating metal nanowires [19–21], templates for creating C [22, 23] or TiO_2 [24, 25] nanotubes, nanoparticle sized ultra active catalysts or supports [11–13], etc. Their optimal effectiveness depends on their suitably designed, porous structure, nature/composition of pore wall oxide and reactive properties. These films are formed in phosphoric, oxalic, chromic, and sulphuric acid solutions [2, 3, 26, 27]. Also, bisulphates [28, 29] and mixtures of H_2SO_4 with sulphate salts were used [28, 30–35]. H_2SO_4 has been employed most frequently. The structure of uniformly/regularly grown films is defined by the surface density of pores, diameter at their bases and real shape of pores.

The films formed in H_2SO_4 have a surface pore density of the order 10^{10} or 10^{11} cm^{-2} [12, 30], depending solely on, and reduced with, current density [30, 36]. The pore base diameter varies from several nm to a few ten nm [30] depending on, and increasing with, temperature and H^+ activity at pore bases [28, 29]. The pores generally open towards the surface due to chemical dissolution of pore walls by the electrolyte during anodising [2, 37–41], similar to open circuit dissolution [37–41]. It is a first order reaction with respect to H^+ activity and is hindered by incorporated electrolyte anions [28]. At prolonged anodising due to pore opening [42, 43] a quasi-maximum limiting thickness may appear [2, 3, 42] decreasing with pore density, temperature and H^+ activity.

Conditions like low temperatures and electrolyte concentrations and high current densities in which, in addition, condensed $Al_2(SO_4)_3$ is not formed inside pores, favour the growth of low porosity hard films [2, 3]. Sulphate additives like Na_2SO_4, $Al_2(SO_4)_3$, $MgSO_4$, $MnSO_4$, $(NH_4)_2SO_4$ and $NiSO_4$ [30–34] were believed to reduce the solvent action of electrolyte, thus favouring hard films. But, actually, their presence may increase the H^+ activity and always increases the concentration of incorporated anions [28, 29, 35]; the first may increase the pore base diameter and rate of pore wall dissolution reaction but the second reduces that rate. Its reduction can prevail in some cases. Conditions as above [43–45] and additives like Na_2SO_4 [30], $Al_2(SO_4)_3$ and $MgSO_4$ [31], etc. also favour pitting appearance due to non-uniform/abnormal growth of films which excessively thicken locally [43–45]. Non-uniform aspect, thickness, porous structure, porosity, hardness and roughness and cracks appear. Hard films and pitting are together favoured [44, 45]. Though hard films with specific structural features seem to be formed in low acidity pure H_2SO_4 baths, against expectations, relevant practices are absent.

Condensed $Al_2(SO_4)_3$ appears as colloidal $Al_2(SO_4)_3$ nanoparticle micelles on the surface of pores [35]. The field at pore base and solid surface of pores catalyse their formation. They appear and disappear according to a quasi-equilibrium process and affect the kinetics and mechanism of film growth by reducing the surface fraction of charge exchange and diameter at pore bases

and the real fraction of wall surface where oxide dissolves; the mechanism of regular film growth is also enhanced. Their coagulation is prevented by their similar charge. Saturated H_2SO_4 + $Al_2(SO_4)_3$ baths exert maximal such effects. The study of Al anodising in saturated baths H_2SO_4 15–105% w/v [46] revealed many details of critical role of micelles and conditions inside pores.

The solubility of $Al_2(SO_4)_3$ decreases with H_2SO_4 concentration up to 95% w/v [35]. Saturated low acidity baths must have Al^{3+} and SO_4^{2-} concentrations close to the highest possible ones. The research of Al anodising in low acidity baths appears interesting especially that concerning: (1) the mechanism of film growth in low acidity H_2SO_4 solutions either pure or saturated; (2) the comparison of growth mechanisms and structural features of films to explain the heretofore non use of low acidity baths; (3) predictions to optimise the process as regards the conditions of regular film growth and certain structural features at low acidity. This is the new idea of this study. A combined overall kinetic/chronopotentiometric method was applied that can effectively discover this mechanism since other methods applied i.e. to barrier type films are ineffective, inaccurate or inapplicable due to the existence of pores [28, 35, 46].

Experimental

For preparing the anodising solutions H_2SO_4, 95–97% w/w (Merck, pro analysi), and $Al_2(SO_4)_3.18H_2O$ (Merck, extra pure, purity ≥99.5777%, 2% aqueous solution of which has a pH≈2.5–4.0) reagents were used. The solubility of $Al_2(SO_4)_3$ in H_2SO_4 solutions at H_2SO_4 concentrations 0 and 5% w/v (0.51 mol dm^{-3}) at 25 °C was first determined as previously [35] described; it was ≈1.05 and 0.98 mol dm^{-3}, respectively. The anodic oxidation of Al was performed galvanostatically in thermostated and vigorously agitated saturated 1 dm^3 $Al_2(SO_4)_3$ solution as well as in that solution acidified by dense H_2SO_4, 95–97% w/w, to H_2SO_4 concentration ≈1.55% w/v. The anodising conditions were temperature 25 °C, current density 15 mA cm^{-2} and time 15 min which in cases of pitting growth is sufficient for its development and easy detection [43, 44]. Though the $Al_2(SO_4)_3$ solubility decreased with H_2SO_4 concentration, to assure saturated bath irrespective of any slight change of its composition and temperature in subsequent experiments, a small amount of $Al_2(SO_4)_3$ was added, 0.05 mol, which did not change appreciably the volume of solution; the $Al_2(SO_4)_3$ content, thus, reached ≈1.1 mol dm^{-3} . The acidification and anodising in the above conditions continued at different steps up to H_2SO_4 concentration ≈3% w/v. Finally, a current density of 35 mA cm^{-2} was also employed. The method of acidification with small amounts of dense H_2SO_4, 95–97% w/w, was adopted to: (1) obtain desired H_2SO_4 concentrations or pH's; (2) bypass difficulties in determining $Al_2(SO_4)_3$ solubility in H_2SO_4 solutions of low concentrations, between 0 and 5% w/v since it must vary imperceptibly; (3) easily prepare saturated solutions at low H_2SO_4 concentrations.

Anodic oxidation of Al was also performed in saturated H_2SO_4 0.51 mol dm^{-3} + $Al_2(SO_4)_3$ 0.98 mol dm^{-3} solution at the above temperature and current densities and different times up to 140 min and in pure H_2SO_4 solutions 1, 2 and 3% w/v at 15 min and 5% w/v at different times up to 160 min.

The added $Al_2(SO_4)_3$ in amounts 1.05 or 1.1 mol dm^{-3} for saturated solutions of H_2SO_4 up to 3% w/v and 0.98 mol dm^{-3} at 5% w/v, was slightly higher than the saturation one. The small amount of precipitate could not appreciably hinder stirring of bath but, in turn, it always assured saturated solution. The pH of solutions at 25 °C was measured before and after each anodising run in each separate condition at one or different anodising times.

Al sheets 0.5-mm thick and 99.5% pure were used. The composition of Al, shape and dimensions of Al anodes and Pb cathodes used and the procedure for washing and neutralizing Al specimens after anodising to remove H_2SO_4 and $Al_2(SO_4)_3$ from the pores and their drying were described earlier [35, 42].

The anodising of Al was also followed chronopotentiometrically. During galvanostatic anodising in saturated baths and film thickening, after some time interval from the start characterised by certain details (see later), the anodic potential required to keep constant current always increases [35]. As verified this potential, determined as previously [47], which almost coincides with the potential drop from the double layer at pore bases to the oxide | metal interface [28, 35], is close to the anodising voltage. For convenience, the latter was recorded. The required voltage increase, also met here, continued up to ≈50 V; then, anodising was interrupted.

The masses of films, necessary for the overall kinetic study, were determined as previously [43]. All anodised Al specimens were examined macroscopically and microscopically to verify the growth or not of pitting or burning (advanced, dark colour, black pitting) as described earlier [44] and occurrence of other phenomena.

Results

General observations for the anodising process, related phenomena and film morphology

The results appear in Table 1. The successive lines represent steps of experiments and observations. The numbers in parentheses show the bath obtained after the step corresponding to this number; d means dense H_2SO_4 (95–97% w/w); pH_{in} and pH_{fi} are the pH's before and after anodising; j is the current density; t is the time of anodising at temperature (T) = 25 °C; $C_{a,0}$ is the (estimated) H_2SO_4 concentration, P and B mean the appearance of pitted or burnt surface regions and S means the development of an $Al_2(SO_4)_3$ salt deposit

Table 1 Conditions of anodic oxidation of Al and observations concerning the appearance of pitting, P, burning, B, and salt deposition on the pitted and burnt regions of specimens, S, in both saturated and pure acid solutions

Number of experimental step	Bath composition	pH_{in}	j/mA cm^{-2}	t/min	pH_{fi}	Estimated $C_{a,0}$, % w/v	Appearance of P, B and S
1	$Al_2(SO_4)_3$ 1.05 mol dm^{-3}	2.331	15	15	2.387	0	Macroscopic P and B, S
2	(1) + 8.1 ml d. H_2SO_4 per dm^3 of solution	1.180	15	15	1.189	1.55	Macroscopic P and B, S
3	(2) + 0.05 mol $Al_2(SO_4)_3$ per dm^3 of solution (total 1.1 mol dm^{-3} $Al_2(SO_4)_3$)	1.245	–	–	1.245	1.55	–
4	(3) + 3.8 ml d. H_2SO_4 per dm^3 of solution	0.708	15	15	0.699	2.10	Macroscopic P and B, S
5	(4) + 1.4 ml d. H_2SO_4 per dm^3 of solution	0.601	15	15	0.595	2.35	Macroscopic P and B, S
6	(5) + 3.5 ml d. H_2SO_4 per dm^3 of solution	0.411	15	15	0.410	2.97 ≈ 3	Macroscopic P or B, S
7	(6)	0.410	35	15	0.412	2.97 ≈ 3	Very intense macroscopically observed P and B, S
8	$Al_2(SO_4)_3$ 0.98 mol dm^{-3} + H_2SO_4 0.51 mol dm^{-3}	0.043	15	Various t's ≤ 140 min	0.062	5.0	Microscopically well observed and macroscopically just observed P
9	(8)	0.062	35	Various t's ≤ 54.45 min	0.081	5.0	Macroscopically observed P, small area S.
10	H_2SO_4 0.102 mol dm^{-3}	1.180	15	15	1.190	1.0	Macroscopic P and B
11	H_2SO_4 0.204 mol dm^{-3}	0.753	15	15	0.758	2.0	Macroscopic P and B
12	H_2SO_4 0.306 mol dm^{-3}	0.601	15	15	0.602	3.0	Macroscopic P and B
13	H_2SO_4 0.51 mol dm^{-3}	0.411	15	Various t's ≤ 160 min	0.435	5.0	Microscopically observed P
14	H_2SO_4 0.51 mol dm^{-3}	0.435	35	15	0.439	5.0	Macroscopic P and B

layer on the pitted or burnt regions. The noted $Al_2(SO_4)_3$ concentration ($C_{s,0}$) almost equals, actually it is imperceptibly higher than, the saturation one ($C_{s,s}$). The citation of photographs/microphotographs of pitted surfaces for all $C_{a,0}$'s employed is unnecessary as they were similar to those given earlier [43, 44], adding no new information.

The following observations derived from Table 1 and additional ones were made.

1. The addition of acidifying H_2SO_4 up to pH's 1.180, 0.601 and 0.411 (i.e. the pH's of pure H_2SO_4 1, 3 and 5% w/v solutions) yielded H_2SO_4 concentrations different than the corresponding ones in pure acid solutions; the presence of salt alters the acidity of solution, apparently due to its acidic character, the lower enough real H_2O concentration and the effect of salt on the equilibrium processes.
2. The anodising process does not affect appreciably the pH and $C_{a,0}$ of solution during a few experiments.
3. The solution of $Al_2(SO_4)_3$ alone, without adding H_2SO_4, is acidic and anodic oxidation of Al well takes place in this solution; nevertheless, it is accompanied with the development of strong pitting in the form of P and B.
4. At $C_{s,0} = C_{s,s}$ and $C_{a,0} = 0$–5% w/v pitting appears. At identical j's and t's (or mean film thicknesses) pitting weakened with $C_{a,0}$ and at $C_{a,0} = 5\%$ w/v it was just detected at the lower j occupying negligible surface area, estimated to be <1%. At identical t, pitting in steps 7 and 9 was much stronger than in 6 and 8; thus the rise of j reinforces growth of pitting. It became stronger with t, at least for $C_{a,0} \leq 3\%$ w/v where it was clearly observed.
5. At $C_{s,0} = 0$ and $C_{a,0} \leq 5\%$ w/v pitting also appeared reinforced with increasing t and j and decreasing $C_{a,0}$; at $j = 15$ mA cm^{-2} and $C_{a,0} = 5\%$ w/v it was just microscopically detected. The results at $C_{s,0} = 0$ and $C_{s,0} = C_{s,s}$ and constant either pH or $C_{a,0}$ and t showed that the addition of $Al_2(SO_4)_3$ at $C_{s,0} = C_{s,s}$ reinforces pitting, unlike the case $C_{a,0} \geq 15\%$ w/v [35, 46]. The differences decayed with $C_{a,0}$ and at $C_{a,0} = 5\%$ they became inappreciable.
6. Condensed $Al_2(SO_4)_3$ salt deposit, like fractals, appeared just above the P or B regions, clearly observed after anodising, that was removed during the washing of specimens. This is consistent with the higher rates of anodic oxidation of Al and production of $Al_2(SO_4)_3$ in the pitted surface, which is smaller than the rest [44], due to the "field assisted" pore base oxide dissolution [2, 3, 30, 32–34, 48–50] and pure chemical wall dissolution [2, 37–41].

Chronopotentiometric study

The plots of required anodising voltage (ΔV) versus t at $C_{a,0}=5\%$ w/v, $C_{s,0}=0$ and $C_{s,0}=C_{s,s}$ are given in Fig. 1a. The ΔV increased abruptly up to a high value depending on $C_{a,0}$ and j in a time of the order of 1 s that marks the nucleation of pores. During a next short transient stage of the order of 1 min it decreased up to a time $t(\Delta V'_m)$ at which ΔV becomes minimum $(\Delta V'_m)$. In this stage, a quasi-steady state pore base diameter, nature/composition of barrier layer and electrolyte composition inside the pores are established. After the initial transient at $C_{s,0}=0$ the ΔV on average decreases slightly (or remains almost constant) with t while at $C_{s,0}=C_{s,s}$ a minimum, ΔV_m, appears at $t=t(\Delta V_m)>t(\Delta V'_m)$ of the order of ten or of several ten min and at $t>t(\Delta V_m)$ it increases initially slightly and later strongly. At the other $C_{a,0}$'s ΔV varied with t up to the t's employed similarly as above; it also increased with j and decreased with $C_{a,0}$ in both cases. At $C_{a,0}$'s $\leq$ 3% w/v in both cases pitting was strong enough, the mechanism of film growth deviates strongly from that of regular one and the t employed was relatively small; thus, citation of relevant chronopotentiometric curves was judged unnecessary as it added no new information. But at $C_{a,0}=5\%$ w/v pitting was weak enough and comparable in both cases; the mechanism of film growth approaches that of regular one and their citation yields much important information (see later).

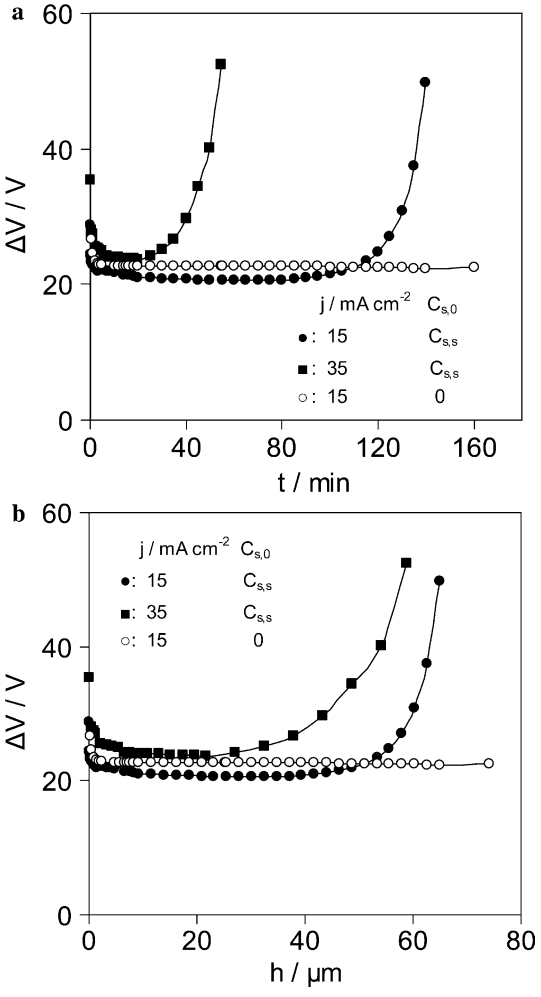

Fig. 1 Variation of the anodising voltage, ΔV, with time, t, (**a**) and film thickness, h, (**b**) at H_2SO_4 concentration $C_{a,0}=5\%$ w/v, current densities $j=15$ and 35 mA cm^{-2} and in saturated H_2SO_4 solution, $C_{s,0}=C_{s,s}$, and pure H_2SO_4 solution, $C_{s,0}=0$

The thickness of uniformly/regularly grown films or the average one of irregular films (h) is given by

$$h = k't = k''jt,\ (t \leq t_l), \tag{1}$$

where k'' is a constant 3.09×10^{-6} cm^3 mA^{-1} min^{-1} and t_l is the time up to which h increases linearly with t [42]. The t_l is identical to, or slightly higher than, t_m that is the time at which the maximum average diameter of pores at a position along them, usually at or near film surface, approaches first the cell width (D_c). At t_m the surface appearance starts to change from a shiny, transparent and similar to Al metal to a mat, milky one [42–44]. For $t>t_l$ h increases with retarded rate with t up to a $t=t_c$ where it may become $\approx$0; then a quasi-maximum limiting h may be achieved exceeding slightly or appreciably $k''jt_m$ or $k''jt_l$ [42, 43]. All t's employed at $C_{a,0}=5\%$ w/v were $<t_m$ for the much larger non-pitted surface region; probably this is valid also for the pitted regions since at this $C_{a,0}$ pitting is slight and the rate of h increase does not notably differ from that in the rest surface. Using Eq. 1, ΔV versus h [$h \leq h(t_m)$] plots were constructed, Fig. 1b, which differ in their relative positions from those in Fig. 1a.

Overall kinetic study

For the noted reasons, the kinetics of film growth at $C_{a,0}=5\%$ w/v has a specific significance in relation to the other $C_{a,0}$'s. The plots of film mass (m) spread over the entire anodised geometric surface of Al specimens ($S_g=30.75$ cm^2 [42]) versus t are given in Fig. 2a. The m versus h [$h \leq h(t_m)$] plots are given in Fig. 2b.

At $C_{s,0}=0$ and constant j, when the film growth is regular and the pore base diameter (D_b) remains constant during anodising, met when $Al_2(SO_4)_3$ colloidal micelles are not formed at pore base [35], the ΔV versus t plot shows an almost horizontal plateau for $t>t(\Delta V'_m)$. Then, the kinetic model

$$\begin{aligned} A &= (kjt-m)\left(4^{-1}\pi S_g d_c k' t\right)^{-1} = A_0 + A_1 t + A_2 t^2 \\ &= 4\pi^{-1}p,\ \left[A_0, A_1, A_2 > 0 \text{ and } t\left(\Delta V'_m\right) \leq t \leq t_m\right] \end{aligned} \tag{2}$$

applies irrespective of pore shape [42, 43], where A is a dimensionless factor; k is a constant resulting from Faraday's law; d_c is the density of compact pore wall oxide (3.42 g cm^{-3}) [42]; $A_0=n\,D_b^2$, where n is the surface pore density; A_1 and A_2 are parameters depending on j and T and p is porosity (v/v). The physical meaning

of A is derived from its relation with p that depends on the structural features n and D_b and geometry of pores defined by the process of pore wall dissolution along the pores. The A_1 and A_2 are derived on the basis of complex kinetics of this process and embrace kinetic and geometric parameters [36, 43]. From Eqs. 1 and 2

$$A = A_0 + A'_1 h + A'_2 h^2 = 4^{-1}\pi p,\ \left[A_0, A'_1, A'_2 > 0 \text{ and } h\left[t(\Delta V'_m)\right] \le h \le h(t_m)\right]. \quad (3)$$

For $t = 0$ the model (2) gives $A_0 = 4\pi^{-1} p$ but initially only a barrier layer exists with zero p. Thus, it applies after the t of pore nucleation, which is of the order of 1 s [28], i.e. negligible compared to t's employed. The limitation $t(\Delta V'_m) \le t \le t_m$ always satisfies this condition. The A (or p) is related to basic features like n, D_b, etc. and magnifies the m differences permitting detailed/accurate studies of regular film growth [28, 36, 43].

When at high $C_{a,0} \ge 15\%$ w/v and $t > t(\Delta V'_m)$ ΔV rises significantly with t, a scatter of points is usually observed and the A versus $t\ [t(\Delta V'_m) \le t \le t_m]$ and $h\ [h[t(\Delta V'_m)] \le h \le h(t_m)]$ plots at $C_{s,0} = C_{s,s}$ obey the equation

$$A \approx A_0 + A_1 t + A_2 t^2 = A_0 + A'_1 h + A'_2 h^2 \quad (4)$$

where A_0, A_2 and A'_2 are >0 while A_1 and A'_1 are usually >0 at low j's and gradually become <0 at higher j's and minima appear [35]. Irrespective of pitting appearance or not, colloidal $Al_2(SO_4)_3$ nanoparticle micelles form at least on the pore base surface affecting the mechanism of film growth. The average D_b decreases with t or h [35]. As A_1 (or A'_1) becomes lower, D_b decreases faster with t or h and/or the average rate of chemical pore wall dissolution decreases, both due mainly to the increase of surface fraction occupied by micelles. Only in this case reduction of p with t or h can be observed. Also in this case $A_0 = nD_b^2$, where now D_b is the steady state one for $t \to 0$ and A_1 and A_2 additionally embrace the deviation of D_b's at $t > 0$ from the above steady state one.

The A versus t and h plots are given in Fig. 3a and b. Figures 1 and 3 show that at $C_{s,0} = 0$ the A versus t and h

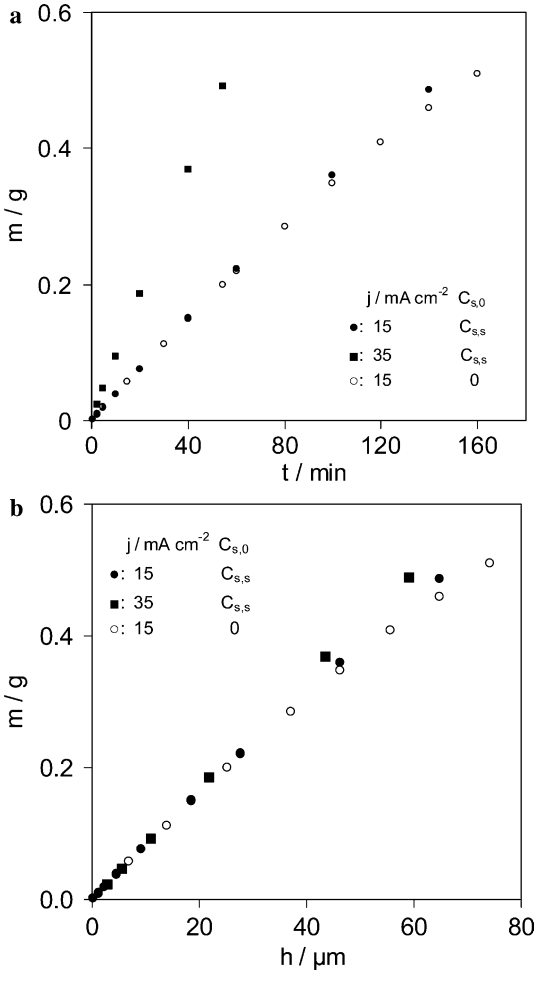

Fig. 2 Variation of the film mass, m, with time, t, (**a**) and film thickness, h, (**b**) at H_2SO_4 concentration $C_{a,0} = 5\%$ w/v, current densities $j = 15$ and 35 mA cm^{-2} and in saturated H_2SO_4 solution, $C_{s,0} = C_{s,s}$, and pure H_2SO_4 solution, $C_{s,0} = 0$

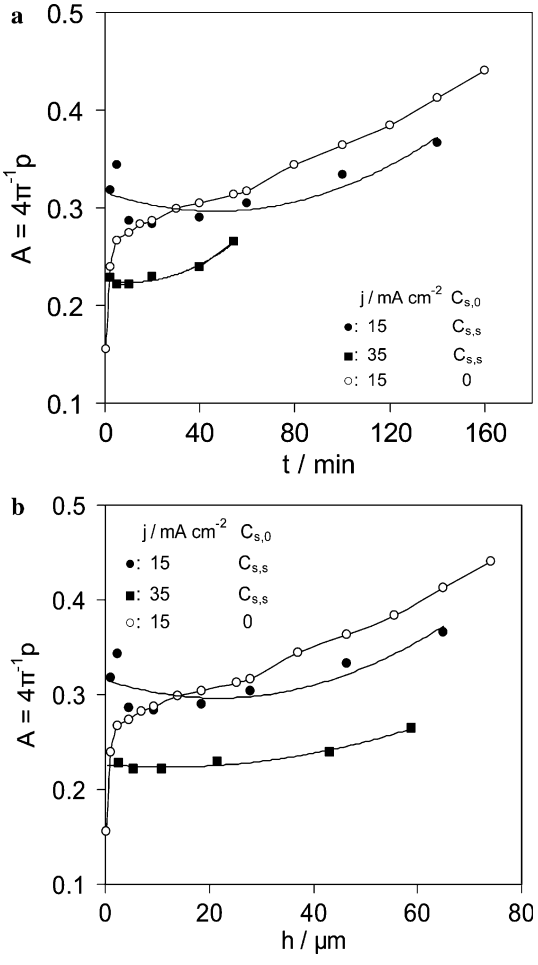

Fig. 3 Variation of the dimensionless factor A with time, t, (**a**) and film thickness, h, (**b**) at H_2SO_4 concentration $C_{a,0} = 5\%$ w/v, current densities $j = 15$ and 35 mA cm^{-2} and in saturated H_2SO_4 solution, $C_{s,0} = C_{s,s}$, and pure H_2SO_4 acid solution, $C_{s,0} = 0$

plot profiles deviate strongly from that predicted by Eqs. 2 and 3 while the appearance of colloidal micelles is excluded. The other plots show growth of micelles; the Eq. 4 gave for $C_{s,0} = C_{s,s}$ $A_0 = 0.3156$, $A_1 = -8 \times 10^{-4}$ min^{-1} and $A_2 = 9 \times 10^{-6}$ min^{-2} at $j = 15$ mA cm^{-2} and $A_0 = 0.2262$, $A_1 = -5 \times 10^{-4}$ min^{-1} and $A_2 = 2 \times 10^{-5}$ min^{-2} at $j = 35$ mA cm^{-2} . At $j = 15$ mA cm^{-2} the A (or p) for low h's is higher at $C_{s,0} = C_{s,s}$ than at $C_{s,0} = 0$ but beyond some h the trend is reversed. The span of A variation is smaller at $C_{s,0} = C_{s,s}$ than at $C_{s,0} = 0$.

As verified at $j = 15$ mA cm^{-2} and $t = 15$ min, m decreased and A increased with $C_{a,0}$ in both cases, $C_{s,0} = 0$ and $C_{s,0} = C_{s,s}$, while the m and A values at $C_{s,0} = C_{s,s}$ were, respectively, lower and higher than those at $C_{s,0} = 0$. Citation of numerical results has no significance, but these trends show that the A versus t plots at lower $C_{a,0}$'s may be qualitatively similar to those at $C_{a,0} = 5\%$ w/v and shifted on average downwards as $C_{a,0}$ decreases.

Derivation of basic features of nanostructure

Since at $j = 15$ mA cm^{-2} $n = 1.269 \times 10^{11}$ cm^{-2} [12] and the ratio of n's at $j = 15$ and 35 mA cm^{-2} is 1.31 [36], at the latter j the mean $n \approx 9.687 \times 10^{10}$ cm^{-2} . The average $D_b = (A_0/n)^{1/2}$ for $h \rightarrow 0$ is $\approx$15.8 and 18.1 nm, i.e. of nm scale. It is not notably affected by j; the slight difference is attributed mainly to rise of temperature at pore bases that is enhanced with j (see later). Since $nD_c^2 = 4/3$ [47], the mean D_c is $\approx$32.4 and 37.1 nm, respectively.

Discussion

The overall processes and conditions inside the pores during the growth of film in low acidity baths

The phenomena inside the pores during Al anodising are complex, determining each other, and greatly affect the mechanism of film growth. For a satisfactory interpretation of results in low acidity baths, as here, the processes and conditions inside pores must be first discussed.

Overall processes occurring inside the pores

The oxide is formed in the oxide/Al interface, Fig. 4, according to Faraday's low [47, 51]. The Mass balance of anodic processes shows that H_2O is consumed yielding O^{2-} for oxide production in amounts corresponding to pore walls around pore bases and H^+ ions released at pore bases [28, 52] ($2Al + 3H_2O - 6e^- \rightarrow Al_2O_3 + 6H^+$). $Al_2(SO_4)_3$ is formed by the "field assisted" pore base surface oxide dissolution [2, 3, 30, 32–34, 48–50], actually through the rejection and then hydration of Al^{3+} and migration of O^{2-} inwards barrier layer [28]. It is formed also by the chemical pore wall oxide dissolution [2, 37–41] ($Al_2O_3 + 3H_2SO_4 \rightarrow Al_2(SO_4)_3 + 3H_2O$). It enters the pore filling solution which, even at $C_{s,0} = 0$, contains $Al_2(SO_4)_3$. The rate of oxide formation exceeds that of dissolution. The rate of H_2O consumption exceeds that of its production and H_2O (together with anions) rushes inwards the pores, filling them; this process occurs, up to the achievement of the maximum possible h or m [42, 43] at $t \geq t_c$, when it really occurs, where the rates of oxide production and dissolution become identical.

The heat evolved during Al anodising, mainly around pore bases, that increases with j and ΔV is dissipated to the bath solution mainly through the pore filling solution, which has higher thermal conductivity than the oxide. A gradient of temperature is set up along the pores [42]. That around pore bases (T_b) is higher than T and that at position x, Fig. 4, (T_x) decreases towards the pore mouths. The $T_x - T$ increases with x, j and ΔV and decreases with T and diameter at position x (D_x) [42]. The $C_{a,0}$ and $C_{s,0}$ may secondarily affect T_b and T_x. After transient phenomena end, at each t and x a quasi-steady state is attained for mass, charge and heat transfer.

Steady-state conditions inside the pores during regular and irregular film growth at low $C_{a,0}$'s and both $C_{s,0} = C_{s,s}$ and $C_{s,0} = 0$

As shown at $C_{a,0} \geq 15\%$ w/v and $C_{s,0} = C_{s,s}$ supersaturation dominates inside pores during film growth,

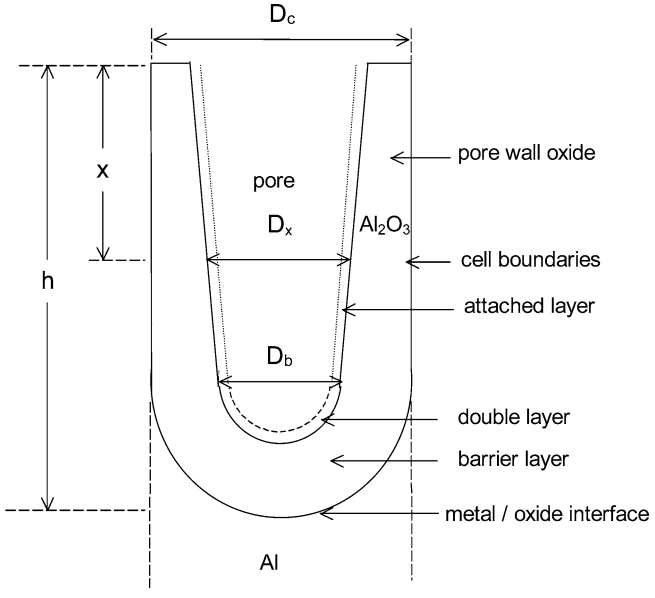

Fig. 4 Schematic representation of a section parallel to the pore axis of an elongated, columnar cell of a porous anodic alumina film. The pore, the pore base diameter D_b, the pore diameter at a position x along the pores D_x, the cell size D_c, the pore wall oxide and the hemispherical shell shaped barrier layer are distinguished. Also, the metal | oxide interface and the cell boundaries are shown. The pore generally broadens towards the film surface as a result of the pore wall chemical dissolution reaction by the electrolyte inside the pores during the film growth

which is enhanced towards the pore base and as j increases and T_x decreases [46]. The concentration of H_2SO_4 varies slightly along the pores and that of $Al_2(SO_4)_3$ increases towards the bases of pores. This is valid also in the present case since there is no conceived reason for the opposite. Also at each j and h, the average D_x is lower (see later), ΔV is higher and thus $T_b - T$ and $T_x - T$ are larger than at higher $C_{a,0}$'s [46]. Supersaturation favours the growth of $Al_2(SO_4)_3$ micelles on the surface of pores but the rise of T_b and T_x acts oppositely [35, 46].

The study of quasi-steady-state transport phenomena inside the pores during anodising of Al in H_2SO_4 solution considering regular film growth and $T_x = T$ [44, 52] showed that the dependence of acid and $Al_2(SO_4)_3$ concentrations around pore bases ($C_{a,b}$ and $C_{s,b}$) and at position x along the pores, Fig. 4, ($C_{a,x}$ and $C_{s,x}$) on h, x, j, T and $C_{a,0}$ is generally very complex. In the region of low $C_{a,0}$'s and the T employed here, the study of transport phenomena [44] showed that at $C_{a,0} = 1\%$ w/v and lower j $C_{a,x}$ decreases up to a few ten μm and then rises slightly with x while at $C_{a,0} = 5\%$ w/v $C_{a,x}$ decreases slightly up to the x or $h = 150$ μm examined. At the higher j and both $C_{a,0}$'s, $C_{a,x}$ decreases slightly with $\times$ in a region of a few μm and then strongly rises. The $C_{a,x} - C_{a,0}$ varies with j by a complex way depending on h, $C_{a,0}$ and T. The concentration and activity of H^+ in the bath solution ($C_{H+,0}$, $a_{H+,0}$), at position x along the pores ($C_{H+,x}$, $a_{H+,x}$) and at pore bases ($C_{H+,b}$, $a_{H+,b}$) must follow $C_{a,0}$, $C_{a,x}$ and $C_{a,b}$. The $C_{s,x}$ increases with x and j, decreases with T and imperceptibly changes with $C_{a,0}$ [44].

At the employed T and low h's, the $C_{a,b} - C_{a,0}$ passes through a minimum at $j \approx 15$ mA cm^{-2} for $C_{a,0} = 1\%$ w/v and at $j \approx 20$ mA cm^{-2} for $C_{a,0} = 5\%$ w/v [44]. These are the critical j's (j_c) above which pitting appears, defined by ($h \rightarrow 0$) $\partial C_{a,b}/\partial j = 0$ [44, 45] or $\partial a_{H+,b}/\partial j = 0$ [53]. For both $C_{a,0}$'s and the higher j employed, the growth of pitting is justified, as indeed observed. But inconsistencies appear for the lower j at $C_{a,0} = 1\%$ w/v where just detected pitting could at most appear, while, actually, it is strong, and at $C_{a,0} = 5\%$ w/v where it should not appear, but, really, slight pitting appears. They mark a peculiar behaviour rather than experimental errors or some effect of T_b. At each h, $T_x - T$ must be also notable due to the relatively high ΔV's.

In both cases $C_{s,0} = 0$ and $C_{s,0} = C_{s,s}$, the pitted surface generally gradually enlarges, the rest shrinks and the average j's are re-arranged in the two regions, initially fast and then slowly until a pseudo-steady state is attained. Also changes in the composition of pore filling solution and T_x and their distribution along the pores occur [44]. The differences in local h, D_b, barrier layer thickness, T_b and distributions of electrolyte composition and T_x in pores, which vary with t, predict a chaotic, non-linear behaviour characterised by loops of effects of different parameters especially for strong pitting [44]. A strict analysis of conditions inside pores, as in regular growth [44, 45, 52], and interpretation of overall kinetic data is thus prohibited. A qualitative only description is possible in view of dependence of conditions in pores on j, T, h, etc. for regular growth. Thus, e.g. h and T_b are higher in pitted regions; but $C_{a,x}$ and $C_{s,x}$ may be lower or higher affected by the different local j, T_x and h.

Interpretations of results and peculiar characteristics of film growth mechanism

Interpretation of ΔV versus t or h plots and their relative positions and of ΔV variation with $C_{a,0}$, $C_{s,0}$ and j

Figure 1 shows that at $C_{s,0} = C_{s,s}$ after the transient, ΔV varies slightly with t up to a high t or h forming a plot plateau with a slight minimum and then rises. This behaviour differs from that at higher $C_{a,0}$'s, e.g. 15% w/v, $C_{s,0} = C_{s,s}$ and $j = 15$ mA cm^{-2} where after the initial transient, ΔV notably rose in a large t range and later it rose strongly while at $j = 35$ mA cm^{-2} ΔV rose strongly immediately after the transient [35]. The increase of $C_{s,b}$ enhances the growth of micelles rising the fraction of occupied pore base surface. The increase of T_b acts oppositely [35]. Supersaturation in pores favours maximal growth of micelles at each h. The low acidity of bath results in low D_b and large thickness of barrier layer $2^{-1}(D_c - D_b)$ which requires high ΔV notably rising T_b. At each j, D_b [36] increases and $2^{-1}(D_c - D_b)$ decreases with T_b reducing ΔV. Both T_b and $C_{s,b}$ increase with h. The effect of rising T_b is initially larger than that of $C_{s,b}$; later the trend is reversed. Thus, ΔV decreases up to $t(\Delta V_m)$ and then an accelerated increase is observed due mainly to the rise of the above surface fraction and decrease of D_b with h [35]. Micelles are not formed at $C_{s,0} = 0$ and a plateau appears in ΔV versus t plot for all t's $> t(\Delta V_m$'), where ΔV slightly decreases with t due to some rise of T_b slightly increasing D_b and reducing $2^{-1}(D_c - D_b)$.

The ΔV generally decreased with $C_{a,0}$ at both $C_{s,0} = C_{s,s}$ and $C_{s,0} = 0$. The average n and D_c depend only on j [36] and are almost identical but the D_b increases with $a_{H+,\,b}$ [28] that follows $C_{a,b}$ or $C_{a,0}$; $2^{-1}(D_c - D_b)$ decreases reducing ΔV [28]. The higher ΔV at $C_{s,0} = 0$ than at $C_{s,0} = C_{s,s}$ in plots plateau for identical j, Fig. 1, is explained by that the average D_b is lower, following $a_{H+,b}$ [28], while D_c is almost identical; thus, $2^{-1}(D_c - D_b)$ is larger at $C_{s,0} = 0$ requiring higher ΔV [28], irrespective of any effect of micelles on ΔV at $C_{s,0} = C_{s,s}$. Beyond the plateau, at $C_{s,0} = C_{s,s}$ the surface fraction occupied by micelles increases, D_b decreases and ΔV gradually exceeds that at $C_{s,0} = 0$. At $C_{s,0} = C_{s,s}$ and each h ΔV increases with j since, irrespective of the effect of $2^{-1}(D_c - D_b)$ value and double layer on ΔV, the average field strength across the barrier layer and that surface fraction increase with j [28, 35].

Real conditions inside the pores establishing a long initial transient stage at low $C_{a,0}$'s and $C_{s,0}=0$; interpretation of the A versus t or h plots and of pitting appearance conditions

At $C_{s,0}=0$, $j=15$ mA cm^{-2} and $h \rightarrow 0$, $nD_b^2 \approx 0.15$, Fig. 3, and $D_b \approx 10.9$ nm. The growth of film starts as regular and later it becomes irregular [44]. In the quasi-steady state, this j and $T=25$ °C, the equation [28]

$$\left(nD_b^2\right)^{-1} = 0.3947 a_{H+,b}^{-1} + 2.2645 \quad (5)$$

is valid for regular growth. For $h \rightarrow 0$ $a_{H+,b}$ is found 0.090 that is small enough compared to $a_{H+,0}=10^{-pH}=0.388$. Such a drop of acidity is not predicted by the quasi-steady state transport analysis [44]. The conditions inside the pores in the first stage of strong increase of A with t deviate strongly from the quasi-steady state ones. This must be a long transient stage where the acidity at pore bases becomes low enough or H^+ ions are almost depleted. The validity of this suggestion is tested below: In conditions close to steady state ones, pitting is just detectable and equation (2) must roughly apply. If the results beyond the long transient, i.e. for $t>30$ min, are considered, then A_0 is ≈ 0.29. Adopting that $a_{H+,0} \approx a_{H+,b}$, from Eq. 5 $nD_b^2 \approx 0.30$ that is close to 0.29; then the steady state D_b is ≈ 15.4 nm. If, as expected, the depletion of H^+ is stronger on decreasing $C_{a,0}$, the transient region of the A versus t or h plots must become larger. Earlier A versus t plots results at $C_{a,0}=2$ and 3% w/v [43] exactly confirmed it.

The double layer on the pore base surface consists of the fixed layer, containing mainly SO_4^{2-} [28] and the diffuse layer, containing all ions. Al^{3+} and H^+ are rejected from that surface, traverse the fixed layer and drop in the diffuse layer where they become hydrated. The concentrations of cations and positive charge must increase towards the boundary of diffuse layer and pore filling solution where almost electroneutrality is first attained; the concentrations of SO_4^{2-} and HSO_4^- and negative charge accordingly decrease. The hydration number of Al^{3+} is high, 26 on average [54], consistent with the high hydration enthalpy. The diameter of hydrated ion group must be at least that of a sphere consisting of 26 H_2O molecules, assuming that the small size of Al^{3+}, with radius ≈ 0.057 nm [54], is compensated by compressive attractive forces. From the molar volume of H_2O, 18 cm^3 mol^{-1}, the diameter of group is found >1.1 nm that is large compared to the non-equilibrium D_b when $h \rightarrow 0$. The hydration enthalpy and number of anions are low [54] and their size is close to that of unhydrated ions.

Beyond the diffuse layer, the current is conducted mainly by cations [55]. For $h \rightarrow 0$ the flux rate of migrating Al^{3+} is low due to low concentration ($\rightarrow 0$) and large size of hydrated Al^{3+} groups; as it approaches D_x, hindrances to their migration may be exerted either mutually or by the attached layer, Fig. 4. At low h's Al^{3+} ions accumulate as h increases, thus increasing $C_{s,x}$ and enhancing hindrances. The migration of H^+ is easier, due to its hopping mechanism; the current is conducted almost solely by H^+. Though the rate of H^+ production at pore bases is higher at lower D_b [46], the concentration of H^+ is low and they are almost depleted, more at lower $C_{a,0}$.

The nucleation of pores may occur in small cracks created by mechanical stresses [28] and destined to become pores. The high acidity deters depletion of H^+ and they are quickly transformed to pores, with D_b close to steady state one, and transient early ends. Low acidity allows almost depletion of H^+ inside pores at low h's. The D_b is small, $2^{-1}(D_c - D_b)$ is large and ΔV is high enough causing the rise of T_b and T_x with h, which result in the gradual increase of D_b and D_x. Also $C_{s,b}$ must increase. At $h>0$ all these gradually increase the flux rate of migrating Al^{3+} and reduce H^+ depletion. These processes continue until the pores widen enough and the transport phenomena, D_b and D_x approach the steady state ones. The transient ends when $C_{H+,b}$ or $a_{H+,b}$ approach $C_{H+,0}$ or $a_{H+,0}$ and distribution of all ions inside pores approaches that given by the steady-state transport analysis [44, 52].

In the quasi-steady state and at h's comparable to the present ones, the $C_{H+,x}$ or $a_{H+,x}$ do not largely differ from $C_{H+,0}$ or $a_{H+,0}$ while as $C_{H+,0}$ or $a_{H+,0}$ decreases, j_c also decreases [44]. In the transient stage and for $h \rightarrow 0$, the $C_{H+,b}$ or $a_{H+,b}$ become much lower than $C_{H+,0}$ or $a_{H+,0}$ so that the real j_c decreases compared to the steady state one. This justifies the growth of pitting at j's not predicted by the steady-state transport analysis. As h increases, $C_{H+,b}$ or $a_{H+,b}$ and j_c increase. Beyond some h, j_c may become $\geq j$, the progress of pitting ends, regular film growth is set up and the pitted regions may be gradually repaired. That's why at $C_{a,0}=5\%$ w/v pitting did not grow enough, but remained just detectable even up to $t=160$ min. The transient in the ΔV versus t or h plots must be also long at low $C_{a,0}$'s, as indeed shown in Fig. 1. But, the transient t range is shorter than that of A versus t or h plots. The first plots concern almost solely the processes in the region from double layer at pore bases to the oxide|metal interface, which may show shorter transients; the second plots concern, besides those, the processes of pore wall dissolution which may show longer transients. The characteristic A versus t or h plot profile at $C_{s,0}=0$ is thus mainly due to the long transient and not to pitting development "per se" which must exert secondary effects.

Interpretation of both the relative positions of A versus t or h plots at different conditions and the strongly different plot profiles at $C_{s,0}=C_{s,s}$ and $C_{s,0}=0$

The higher A's at $C_{s,0}=C_{s,s}$ than at $C_{s,0}=0$ for $h \rightarrow 0$ are due mainly to the fact that, though D_c is comparable, the average D_b is larger in the first case owing to the higher $a_{H+,b}$ [28] that follows $a_{H+,0}$ while D_b in the second case is

further reduced due to the long transient stage that decreases $a_{H+,b}$. At $h>0$, the D_b at $C_{s,0}=C_{s,s}$ gradually decreases and later it becomes even lower than that at $C_{s,0}=0$ in the quasi-steady state for identical t or h due to the growth and effect of micelles which are enhanced with h [35]. The rate of wall dissolution at position x (r_x) depends linearly on both the $a_{H+,x}$ and free surface fraction not occupied by micelles [35]; it also decreases with the concentration of incorporated anions in the pore wall oxide which is much higher at $C_{s,0}=C_{s,s}$ than at $C_{s,0}=0$ [28]. At $C_{s,0}=C_{s,s}$ the higher $a_{H+,x}$ increases r_x and the lower above fraction (<1) reduces it. The second effect and that of anions dominate so that the average r_x is lower at $C_{s,0}=C_{s,s}$. The average gradient of A versus t or h plots and the span of A variation are thus smaller at $C_{s,0}=C_{s,s}$. The plots at this $C_{s,0}$ are shifted downwards with j due to decrease of n [36] and stronger growth of micelles and effect on D_b and average r_x.

The concentrations (and activities) of Al^{3+} and H^+ are higher at $C_{s,0}=C_{s,s}$ than at $C_{s,0}=0$. The Eq. 5 and $a_{H+,0}=10^{-pH}=0.906$ give for the lower j, $nD_b^2\approx 0.37$ that is near $A_0\approx 0.32$ found by Eq. 4; the difference is due to the appearance of micelles which gradually reduce D_b, to some uncertainties owing to the scatter of points in the A versus t or h plots at $C_{s,0}=C_{s,s}$, etc. The A versus t or h plots at $C_{s,0}=C_{s,s}$ do not show detectable transient. But at $C_{s,0}=0$ they include the initial long transient, where A strongly rises with t or h, and the quasi-steady state one. The strongly different A versus t or h plots profiles at $C_{s,0}=0$ and $C_{s,0}=C_{s,s}$ are thus justified.

At the employed T and each j, the average A and the span of A variation here are smaller than those at $C_{a,0}=$ 15–105% w/v for comparable h ranges either at $C_{s,0}=0$ or $C_{s,0}=C_{s,s}$ [43, 46]; this is due to the lower average D_b and r_x (and thus D_x), resulted from the much lower $C_{H+,b}$ or $a_{H+,b}$ and $C_{H+,x}$ or $a_{H+,x}$.

Interpretation of development of salt deposit layer on the pitted regions of Al anode surface

The deposition of salt on the P or B regions was never before observed at $C_{a,0}=15$–105% w/v, $j=15$ mA cm^{-2} and $C_{s,0}=0$ [43], as expected, while at $C_{s,0}=C_{s,s}$ [46] it was occasionally met only at very high j's $\geq$ 105 mA cm^{-2}. As shown here, it is not developed at $C_{a,0}=1$–5% and $C_{s,0}=0$. $Al_2(SO_4)_3$ precipitate is not formed inside the pores [35]. A considerable flux of Al^{3+} from pores to bath solution occurs due to conduction of current almost solely by cations [55] and increase of $C_{s,x}$ with x. In the bath bulk solution the concentrations of Al^{3+} and SO_4^{2-} obey the solubility constant value and are higher while that of H_2O is lower than those at higher $C_{a,0}$'s and $C_{s,0}=C_{s,s}$[46]. The solution is viscous enough and an electrolyte layer is attached on the anode surface. The H_2O required to fill the pores comes from this layer. The concentration of H_2O inside it drops towards the pore mouths and the concentrations of Al^{3+} and SO_4^{2-} accordingly increase. Supersaturation may appear in this layer similarly enlarged. The agitation occurring to some extent inside it may reduce the supersaturation. Salt precipitate appears starting from film surface. Its grains are relatively easily removed by the agitated solution. H_2SO_4 feeds the salt deposition with anions and the cathodic reaction ($2H_3O^+ + 2e \rightarrow 2H_2O + H_2$) with H^+.

The flux of Al^{3+} outwards and H_2O inwards the pores and deposition of salt in the non-pitted surface are slow and all particles of deposit are removed. But in the pitted regions these phenomena are fast, stirring is unable to remove all particles of deposit and some amount is attached on the surface; it increases with t and probably tends to a limit. Though at $C_{a,0}=5\%$ w/v and the higher j employed the deposit was clear, it was not at the lower j due to the small pitted surface, weak pitting, small enough rate of deposit formation and the removal of all its particles. The fact that at $C_{s,0}=C_{s,s}$ and higher $C_{a,0}$'s deposit was observed only at much higher j's [46], is then due to that only at such high j's the concentrations of Al^{3+} and SO_4^{2-} become high and that of H_2O becomes low enough in the layer attached on anode surface so that the conditions resemble the above noted ones.

Interpretation of peculiarities in pitting appearance conditions

In $H_2SO_4+Al_2(SO_4)_3$ electrolytes with identical $C_{a,0}\leq$ 15% w/v and different $C_{s,0}$'s up to that at which micelles do not appear on pore base surface the steady state j_c decreases with $C_{s,0}$ [35]. Then j_c strongly rises with $C_{s,0}$, due to the increase of amount of micelles per unit surface at pore bases that becomes highest at $C_{s,0}=C_{s,s}$. At $C_{a,0}\geq$ 15% w/v, $C_{s,0}=C_{s,s}$ and each T, j_c exceeds that at $C_{s,0}=0$ [35, 46]. But at low $C_{a,0}$'s as here, the opposite is valid. This is rather due to effects of viscous solution on transport phenomena (more than at higher $C_{a,0}$'s), notable T_x-T's, etc. at $C_{s,0}=C_{s,s}$, that reduce the control of film growth by micelles although T_b is larger rising j_c. Pitting is thus stronger at $C_{s,0}=C_{s,s}$ than at $C_{s,0}=0$ where as noted it is ascribed mainly to the initial transient.

For $C_{a,0}=5\%$ w/v and $C_{s,0}=C_{s,s}$ the steady sate and real j_c's coincide and as j decreases pitting weakens. At $j=15$ mA cm^{-2} pitting is just detected; thus this j just exceeds j_c. The difference of steady state j_c's at $C_{s,0}=C_{s,s}$ and $C_{s,0}=0$ shrinks with $C_{a,0}$, since the previous effective factors weaken. At a $C_{a,0}$', just exceeding 5% w/v, they coincide. At $C_{a,0}<C_{a,0}$' and each j pitting is stronger, or the steady state j_c is lower, at $C_{s,0}=C_{s,s}$ but at $C_{a,0}>C_{a,0}$' the trends are reversed, conforming to those at $C_{a,0}\geq 15\%$ w/v [46].

The possibility to optimise the regular film growth in low acidity sulphate baths

The non use of low acidity H_2SO_4 baths in practice to produce low p hard films is due thus to the long transient,

accompanied by the growth of abnormally strong pitting and high ΔV's. The use of saturated baths cancels that long transient. The effect of micelles and incorporated anions gradually dominate over that of their higher acidity at $h \gg 0$ and p becomes lower even than that at $C_{s,0} = 0$. But the steady state j_c may be still higher.

Al anodising at low $C_{a,0}$'s and $C_{s,0} = C_{s,s}$ shows many peculiarities when compared to that at similar $C_{a,0}$'s and $C_{s,0} = 0$ and at $C_{a,0} \geq$ 15% w/v and $C_{s,0} = C_{s,s}$ [35, 46]. During regular film growth, e.g. at $j < 15$ mA cm^{-2}, a behaviour like that in Fig. 3 is expected. The growth of films at high h's with p lower or at low h's with p higher than that at similar $C_{a,0}$'s and $C_{s,0} = 0$ is thus possible. Also films with p lower than that at $C_{s,0} = C_{s,s}$ and higher $C_{a,0}$'s, e.g. $C_{a,0} =$ 15–105% w/v [46], can be formed. At these j's they will have high n and p lower than that at $C_{s,0} = 0$ and high h's and at higher $C_{a,0}$'s and almost all h's. Much higher h's than in other cases, and irrespective of D_b, much higher maximum limiting h's and real surfaces needed in applications like adsorption, catalysis, etc. thus can be achieved. These constitute an optimisation of process that can be further extended by varying T [46].

Conclusions

1. Anodising of Al was performed galvanostatically at constant T in solutions of H_2SO_4, 0–5% w/v, pure and saturated by $Al_2(SO_4)_3$ and studied by chronopotentiometry and overall kinetics. It took place even in pure $Al_2(SO_4)_3$ solution, which was acidic enough. Al anodising in low acidity solutions saturated and pure shows many peculiarities either when these baths or these with higher acidity baths are compared, like differences of porosity and its dependence on film thickness, lower critical current densities above which pitting appears in saturated than in pure acid solutions, salt deposition on pitted surfaces in the first, etc.
2. The different conditions in pores are responsible for these peculiarities. Such differences are supersaturation and higher temperature, due to the needed higher anodic potential, and more viscous solution in saturated baths of low acid concentrations than at high ones, almost depletion of H^+ during a long initial transient stage in similar low concentrations pure acid baths, etc. Saturated low acid concentration baths cancel this transient and prevail as regards the mechanism of growth and structure of low porosity films at specific conditions.
3. Pitting always appeared at the j's employed; it was stronger in saturated than in pure acid solutions and weakened with acid concentration. A threshold $C'_{a,0}$ exists, just exceeding 5% w/v, where the steady-state critical current density j_c is identical for both pure and saturated solutions. At $C_{a,0} < C'_{a,0}$ it is lower for saturated ones but at $C_{a,0} > C'_{a,0}$ the trend is reversed resembling that at $C_{a,0} \geq$ 15% w/v [46]. Optimisation of regular film growth is possible in these baths at j's $< j_c$'s as regards certain structural features, as at higher $C_{a,0}$'s.
4. The present and earlier [35, 46] results, allow the optimisation of conditions to produce regularly grown, uniform, high quality films of desired/designed structure and p varying in large ranges and essentially introduce new technologies. Yet unsolved problems may be solved like the production of regular films with desired low porosity for mechanical applications and protection technologies and high pore surface density, probably pore base diameter, thickness and real surface for applications involving reactivity of material like adsorption, catalysis, etc. Also, they may be used in more recent applications like nanoscience/nanotechnology, etc.

References

1. Leach SL, Neufeld F (1969) Corros Sci 9:225
2. Diggle JW, Downie TC, Goulding CW (1969) Chem Rev 69:365
3. Young L (1961) Anodic oxide films. Academic Press, London
4. Shreir LL (1976) Corrosion, vol. 2. Newnes-Butterworths, London
5. Smith AW (1973) J Electrochem Soc 120:1068
6. Kawai S, Ishiguro I (1976) J Electrochem Soc 123:1047
7. Rai K, Ruckenstein E (1975) J Catal 40:117
8. Chu Y, Ruckenstein E (1976) J Catal 41:384
9. Ihm SK, Ruckenstein E (1977) J Colloid Interface Sci 61:46
10. Ihm SK, Ruckenstein E (1978) IEC Prod Res Dev 17:110
11. Patermarakis G, Pavlidou C (1994) J Catal 147:140
12. Patermarakis G, Moussoutzanis K, Chandrinos J (1999) Appl Catal A:General 180:345
13. Patermarakis G, Nikolopoulos N (1999) J Catal 187:311
14. Bai XD, Heming C, Ma CL, Peng DQ, Duo D, Zhong DX, Lu JF, Guo BH, Xin Z, Bai GM, Guo JL (2004) Rare Met Mater Eng 33:300
15. Mozalev A, Magaino S, Imai H (2001) Electrochim Acta 46:2825
16. Holland ER, Li Y, Abbott P, Wilshaw PR (2000) Displays 21:99
17. Gaponenko NV, Molcham IS, Thompson GE, Skeldon P, Pakes A, Kudrawiec R, Bryja L, Misiewicz J (2002) Sens Actuators A 99:71
18. Patermarakis G, Kerassovitou P (1992) Electrochim Acta 37:125
19. Zhang Z, Gekhtmann D, Dresselhaus M, Ying J (1999) Chem Mater 11:1659
20. Wang Z, Kuok M, Ng S, Fan H, Lockwood D, Nielsch K, Wehrspohn R (2001) Mater Phys Mechan 4:22
21. Gao T, Meng G, Zhan J, Wan Y, Lian C, Fa J, Zhan L (2001) Appl Phys A 73:251
22. Li J, Papadopoulos C, Xu JM, Moskovits M (1999) Appl Phys Let 75:367
23. Che G, Lakshmi B, Fisher E, Martin C (1998) Nature 393:346
24. Michailowski A, Almawlawi D, Cheng G, Moskovits M (2001) Chem Phys Lett 349:1
25. Gong D, Grimes C, Varghese O, Hu W, Singh R, Chen Z, Dickley D (2001) J Mater Res 16:3331
26. Thompson GE, Furneaux RC, Wood GC (1978) Corros Sci 18:481
27. Furneaux RC, Thompson GE, Wood GC (1978) Corros Sci 18:853

28. Patermarakis G, Moussoutzanis K, Chandrinos J (2001) J Solid State Electrochem 6:39
29. Patermarakis G, Chandrinos J, Moussoutzanis K (2001) J Electroanal Chem 510:59
30. Wood GC, O' Sullivan JP (1970) Electrochim Acta 15:1865
31. Fukuda Y, Fukushima T (1983) Electrochim Acta 28:47
32. Mason RB (1956) J Electrochem Soc 103:425
33. Tajima S, Umehara Y (1981) Plat Surf Finish 68:54
34. Tomita S (1981) Alutopia 11(4):15
35. Patermarakis G, Moussoutzanis K (2002) J Solid State Electrochem 6:475
36. Patermarakis G, Moussoutzanis K (1995) J Electrochem Soc 142:737
37. Nagayama M, Tamura K (1968) Electrochim Acta 13:1773
38. Nagayama M, Tamura K (1967) Electrochim Acta 12:1097
39. Nagayama M, Tamura K, Takahashi H (1970) Corros Sci 10:617
40. Diggle JW (1973) Electrochim Acta 18:283
41. Diggle JW, Downie TC, Goulding CW (1970) Electrochim Acta 15:1079
42. Patermarakis G, Lenas P, Karavassilis Ch, Papayiannis G (1991) Electrochim Acta 36:709
43. Patermarakis G, Tzouvelekis D (1994) Electrochim Acta 39:2419
44. Patermarakis G, Moussoutzanis K (2001) Corros Sci 43:1433
45. Patermarakis G, Moussoutzanis K (2002) Corros Sci 44:1737
46. Patermarakis G, Moussoutzanis K (2005) J Solid State Electrochem 9:205
47. Patermarakis G, Moussoutzanis K (1995) Electrochim Acta 40:699
48. O'Sullivan JP, Wood GC (1970) Proc R Soc (London) Ser A 317:511
49. Siejka J, Ortega C (1972) J Electrochem Soc 124:883
50. Neufeld P, Ali HO (1973) J Electrochem Soc 120:479
51. Ono S, Ichinose H, Masuko N (1991) J Electrochem Soc 138:3705
52. Patermarakis G (1998) J Electroanal Chem 447:25
53. Patermarakis G, Moussoutzanis K (2003) Chem Eng Comm 190:1018
54. Antropov L (1972) Theoretical electrochemistry. Mir Publishers, Moscow
55. Patermarakis G (1995) J Electroanal Chem 404:69